NanoAnalysis
An International Journal
Available online at: www.jnanoanalysis.net or www.jnanoanalysis.com

Surface chemistry improvement of carbon nanotube (CNT) supported Fischer–Tropsch nanocatalysts

Ali Karimi[a,*], Ahmad Tavasoli[b], Maryam Davari[b], Ali Mohajeri[a]

[a]Gas research Division, Research Institute of Petroleum Industry, Tehran, Iran
[b]School of Chemistry, College of Science, University of Tehran, Tehran, Iran

Abstract

Functionalization of carbon nanotube (CNT) was performed, during preparation of Fischer–Tropsch synthesis (FTS) via cobalt nanocatalysts, to modify the surface properties of CNT support. Common and functionalized CNT supported cobalt nanocatalysts were prepared using impregnation wetness method with cobalt loading of 15 wt.%. The catalysts were characterized by Brunauer–Emmett–Teller (BET), Fourier transform infrared spectroscopy (FTIR), X-ray diffraction (XRD), temperature program reduction (TPR), H_2 chemisorption, and transmission electron microscopy (TEM) technique. Most of the cobalt particles were homogeneously distributed inside the tubes and the rest on the outer surface of the functionalized CNT. Functionalization of CNT shifted the TPR reduction peaks to lower temperatures, improved the reduction degree, and increased the dispersion of cobalt particles and stability of catalysts. The proposed cobalt catalyst supported on functionalized CNT- (N-doped functionalized CNT) increased the FTS rate (g HC/gcat./hr), and CO conversion (%) from 0.1347, and 30 to 0.235, and 47 respectively, compared to that of the catalyst prepared by impregnation wetness method on common CNT. Catalysts supported on functionalized CNT also showed better stability.

Keywords: Fischer–Tropsch; Carbon nanotubes; Functionalization; Activity; Stability

1. Introduction

The use of non-petroleum sources due to lack of resources and minimize environmental pollution is of great interest nowadays. Accordingly, natural gas is considered as an alternative fuel [1–3]. Fischer–Tropsch synthesis (FTS) (the major part of gas to liquid technology) converts synthesis gas into hydrocarbons with high cetane number, environmentally clean and free of sulfur, nitrogen, aromatic compounds, and heavy metals [4]. Synthesis of hydrocarbons is a polymerization reaction in the presence of a catalyst. In this process, carbon monoxide and hydrogen adsorb on the surface of the catalyst and synthesis hydrogenated compounds which consequently produce hydrocarbons and oxygenates by growth of chains [5-6].

Using novel catalytic materials and controlling the nanoparticles size can enhance the catalytic performance [1-3, 6]. Transition metals are used in this process due to their considerable activity. Among them Co, Fe and Ru presented the highest activity [7]. Cobalt is preferred catalysts in FTs because of its

* Corresponding author; Email: karimial@ripi.ir ; Tel.: 982148252395; Fax: 982144739716

higher activity for FTS selectivity toward linear products, more stability, low activity to water-gas shift (WGS) reaction and low price[8,9].

Obtaining high surface area of catalysts in order to increase catalytic activity and selectivity is a main issue, and depend on particle size and appropriate distance between each particle. This is attained by using support which can affect the performance of the catalyst through electronic interactions and migration effects. The morphology and the nature of catalyst's support such as surface area, porosity, shape, and size are considered to be noteworthy factors in gaining a high dispersion of nanoparticles. These catalysts loaded on a support are influenced by the surface reactivity and the microstructure of the support [10]. Al_2O_3, TiO_2 and SiO_2 are usually used as supports for cobalt, but they are not considered as a best choice [11, 12]. Their major weakness is their intense interaction toward cobalt that leads to the formation of mixed compounds. These compounds lose active phase, furthermore, possessing very high reduction temperatures. One way to overcome this problem is using support such as carbon nanotube (CNT) that has a weak interaction toward metal catalysts. CNT has many unique structural properties and has attracted increasing attention as a novel support media for heterogeneous catalysis [13, 14]. Also CNT-based catalysts have extensive activity and stability in FTS, but lead to decrease the C5+ selectivity and increase the methane production compared to common carriers [15].

The major properties of CNT are their hydrophobic and inert nature. In CNT-supported cobalt catalysts, the strong metal–support interactions are reduced to a large extent [16]. Poor interactions of CNT with the metal particles cause further agglomeration and sintering. It is therefore important to change the surface chemistry of CNT, for example, with the introduction of oxygen or nitrogen containing surface functional groups. Upon functionalization, the hydrophobic CNT turns into more hydrophilic so that the CNT surface becomes more reactive [17-19]. Synthesis of highly dispersed and stable cobalt catalysts requires interaction between the support and the cobalt precursor [20]. Functionalization and pretreatment of the support remarkably influence the interaction between the cobalt and CNT supports [21]. The presence of functional groups on CNT surface gives rise to surface polarity and better interaction with metals, which can act as anchor sites for the metal particles [20, 22-23]. It seems that, formation of functional groups on CNT surface, not only decrease the sintering of cobalt, but also accelerate the hydrogen spill-over effect in the reduction process. This in turn will increase percentage dispersion, reduction degree, stability and performance of these catalysts simultaneously. Consequently, synthesis and testing of different functionalized CNT-supported cobalt catalysts ware the aim of the present study. The focus was on different CNT surface functionalization groups and their beneficial influence on catalyst activity, stability, and selectivity. In most of previous studies, the surface activation by nitric acid was used to generate oxygen-containing functional groups on the CNT. Therefore, in this study CNT was activated by means of other techniques. All catalysts were prepared with 15 wt.% cobalt loading and characterized by XRD, TPR, XRD and H2 chemisorption and at the end were applied to FTS reaction in a fixed bed micro reactor at 220 °C and 18 bar during 144 hr continues test.

2. Experimental

2.1. Support preparation

2.1.1. Preparation and purification of CNT

CNT was synthesized through methane decomposition at 900°C over cobalt- molybdenum nanoparticles supported nanoporous magnesium oxide (Co-Mo/ MgO) by chemical vapor deposition (CVD) method [24]. The reaction of methane decomposition was conducted at atmospheric pressure with a holding time of 30 min. The fresh CNT often contained impurities, such as amorphous carbon, catalyst metals, and fullerene or graphite particles [25-27]. Thus these impurities in CNT are one of the factors preventing access to its significant features and need to be eliminated before the experiments. The purification procedure was done as follows: The pristine CNT sample was added to an 18% HCl solution and mixed for about 16 hr at ambient temperature. The resulting mixture was filtered and washed several times with distilled water until the pH of the filtrate was neutral. In order to achieve to extra- purification, the prepared materials dissolved in 6 M nitric acid for 3 hr at 70°C. After that, the washing step was repeated as mentioned above for the HNO_3 treatment process. The resulting cake was dried at 120°C for 8 hr, and in order to eliminate

the amorphous carbons, the temperature was increased to 400°C for 30 min [24,28]. The purity of the CNT was about 95%, with their diameters and lengths ranging between 10-20 nm and 5–15 μm respectively.

2.1.2. Functionalization of CNT

It is known that CNT has a hydrophobic surface, which is prone to aggregation and precipitation in water in the absence of a dispersant/surfactant. Up to now, many efforts have been made to prepare water-dispersible CNT and numerous methods for chemical functionalization of CNT. Among them, we have chosen three methods for CNT functionalization. In the first method, 1g of pure CNT was added to 150 ml H_2O_2 (30%) and sonicated with the probic sonicator for 15 min. Then, the suspending mixture was put in a vertically held Pyrex reactor (length and diameter of 300 and 160 mm respectively) equipped with a gas sparger. A stream of gaseous ozone was continuously passed through the sample at a rate of 314 ml/min for 4 hr. The unreacted ozone gas from the reactor was scrubbed into a sodium iodide solution (5%) before venting to the atmosphere in a fume hood. The resulting mixture was then filtered over a 0.2 mm polycarbonate membrane, and washed with methanol to remove any remaining H_2O_2. The product was dried in an oven at 120°C for 5 hr [28]. This support was named as F1CNT.

In the second method, in order to introduce N-containing functional groups, the CNT was treated at 400°C for 6 hr in flowing ammonia with a flow rate of 25 sccm (10 vol.% NH_3 in He) [29].To neutralize the ammonia gas, it was scrubbed with 5% hydrochloric acid solution. This support was named F2CNT.

In the third method, 1.8 g pure CNT were dispersed in 150 ml of the mixture of ammonium hydroxide (25 wt.%) and hydrogen peroxide (30 wt%) in ratio 50:50 in a round bottom flask. The flask equipped with a reflux condenser and a magnetic stir bar, was kept at 80°C with vigorous mixing for 5 hr. The resulting mixture was then diluted in water and filtered. Then the solid was washed up to neutral pH and dried in vacuum at 40°C overnight [30]. This support was named F3CNT.

2.2. Catalyst preparation

The above produced functionalized and pristine CNT were used as support for preparation of catalysts. For all the catalysts, the concentrations of cobalt were adjusted at 15wt.%. The catalysts were prepared by impregnation wetness method with aqueous solution of cobalt nitrate ($Co(NO_3)_2.6H_2O$ %99, Merck). After impregnation, the catalysts were dried at 120°C for 2 hr and calcined under argon (Ar) flow at 450°C for 3 hr and slowly exposed to an oxygen atmosphere through oxygen/ argon of 1/200 (v/v) at 150°C, during the cooling step. The catalysts prepared were denoted as C_1 for F1CNT, C_2 for F2CNT, C_3 for F3CNT and C_4 for pristine CNT support.

2.3. Characterization

The FTIR absorption technique for confirming the formation of functional groups was conducted on a Bruker ISS-88. A smooth transparent pellet of 0.5-5 % of CNTs mixed with 95-99.5% Potassium Bromide (KBr), was made and the infrared beam passed through this pellet.

The metal loadings of the calcined catalysts were analyzed by using Varian VISTA-MPX inductively coupled plasma-optical emission spectrometry (ICP-OES) instrument. Surface area, pore volume and pores average diameter of the calcined catalysts was measured using an ASAP-2010 V2 Micrometrics system. The samples were degassed at 200°C for 4 hr under 50 mTorr vacuums and their BET area, pore volume and pore diameter was determined. The morphology of the catalysts was studied by transmission electron microscopy (TEM). Sample specimens for TEM studies were prepared by ultrasonic dispersion of the catalysts in ethanol, and the suspensions were dropped onto a carbon-coated copper grid. TEM investigations were carried out using a Philips CM20 (100 kV) transmission electron microscope equipped with a NARON energy-dispersive spectrometer with a germanium detector. The phases and particle sizes of the crystals present in the catalysts were analyzed by XRD using a Philips Analytical X-ray diffractometer (XPert MPD) with monochromatized Cu/Kα radiation, 2θ angles from 20˚ to 80˚. The Debye–Scherer formula was applied to Co_3O_4 peaks at $2\theta = 36.8^o$, in order to calculate the average particle sizes. The H_2-TPR profiles of the catalysts were performed in order to study the reducibility of the metal species in the catalysts. The calcined catalyst sample (0.05 g) was first purged in a flow of helium (He) at 140°C to remove traces of water and gases exist in catalysts' pores, and then cooled to 40°C. Then the TPR

of each sample was performed using 5% H_2 in Ar stream at a flow rate of 40 ml/min at atmospheric pressure using Micrometrics TPD-TPR 2900 analyzer equipped with a thermal conductivity detector (TCD), heating at a linearly programmed rate of 10°C /min up to 850°C. The amount of chemisorbed hydrogen on the catalysts was measured using the Micromeritics TPD–TPR 290 system. 0.25 g of the sample was reduced under hydrogen flow at 400°C for 12 hr and then cooled to 100°C under hydrogen flow. Then the flow of hydrogen was switched to argon at the same temperature, which lasted about 30 min in order to remove the weakly adsorbed hydrogen. Afterwards, the temperature programmed desorption (TPD) of the samples was obtained by increasing the temperature of the samples, with a ramp rate of 10°C /min, to 400°C under the argon flow. The TPD profile was used to determine the cobalt dispersion and its surface average crystalline size. After the TPD of hydrogen, the sample was reoxidized at 400°C by pulses of 10% oxygen in helium to determine the extent of reduction. It is assumed that Co° is oxidized to Co_3O_4. The calculations are summarized in Ref. [30].

2.4. Reaction testing

Fischer-Tropsch synthesis has been performed in a tubular down flow, fixed-bed reactor system. The reactor was made up of stainless steel tube of 450-mm length and 22-mm inside diameter. Brooks 5850 mass flow controllers were used to add H_2 and CO at the desired rate to the reactor. Typically, 1 g of the catalyst was charged into the reactor. The reactor was placed in a molten salt bath with a stirrer to ensure a uniform temperature along the catalytic bed. The bath temperature was controlled via a PID temperature controller. The catalyst reduced under flowing of hydrogen at 400°C for 12 hr. After the catalyst reduction, the mixed gases (CO and H_2) were fed at a flow of 50 ml/min, a temperature of 220°C, H_2/CO ratio of 2 and pressure of 2 MPa. The products were continuously removed from the reactor and passed through two traps, one maintained at 100°C (hot trap) and the other at 0°C (cold trap). The CO, CO_2 and other gaseous products were monitored with time intervals of 2 hr. The liquid products were collected after completion of the run and analyzed by means of three gas chromatographs, a Shimadzu 4C gas chromatograph equipped with two subsequent connected packed columns: Porapak Q and Molecular Sieve 5A°, and a thermal conductivity detector (TCD) with argon which was used as a carrier gas for hydrogen analysis. A Varian CP 3800 with a Petrocol Tm DH100 fused silica capillary column and a flame ionization detector (FID) were used for liquid products so that a complete product distribution could be provided. A Varian CP 3800 with a chromosorb column and a thermal conductivity detector (TCD) were used for CO, CO_2, CH_4 and other non-condensable gases.

3. Results and discussion

3.1. CNT characterization

Results of FTIR are given in Figure 1. This figure shows the infrared spectrum of the purified nanotubes and functionalized ones. The peak at 1601 cm^{-1} is observed for all of samples due to the stretching mode of double-bonds (C=C) in the nanotube backbone. The coupling of functional groups to CNT can be confirmed by presence of a series of new vibrational bands at 3300-3600 cm^{-1} (OH). Although, the moisture in the sample and KBr pellets in the FTIR sample preparation, increases the intensity of these peaks. Peaks at 1771 cm^{-1} (C=O for carboxyl groups), 1262 cm^{-1} (C–O), 2850-2950 cm^{-1} (both C–H anti symmetric and symmetric stretch for CH_3 and CH_2 are shown [28]. There is a peak at 597 cm^{-1} bands of C-H bending mode. The main reason for this peak is the defects which are formed when the CNT is significantly functionalized. The infrared spectrum of F1CNT and F3CNT show that the peaks of these samples are almost identical to pure CNT except that the related C=O and carbonyl peak intensity are increased, which indicates that further functionalized surface is available. In addition, there is a broad peak at 3360 cm^{-1} in F3CNT that can be attributed to the OH and –NH groups. In spectrum of F2CNT new peaks are appeared. The peak at 1037 cm^{-1} that can be correspond to the –C–N stretching frequency. The broadening of the peak at 3300-3400 cm^{-1} confirms the presence of –NH stretching frequency. A shift in C=O stretching frequency from 1771 cm^{-1} in F1CNT to 1644 cm^{-1} in F2CNT confirms –NH bonds [31].

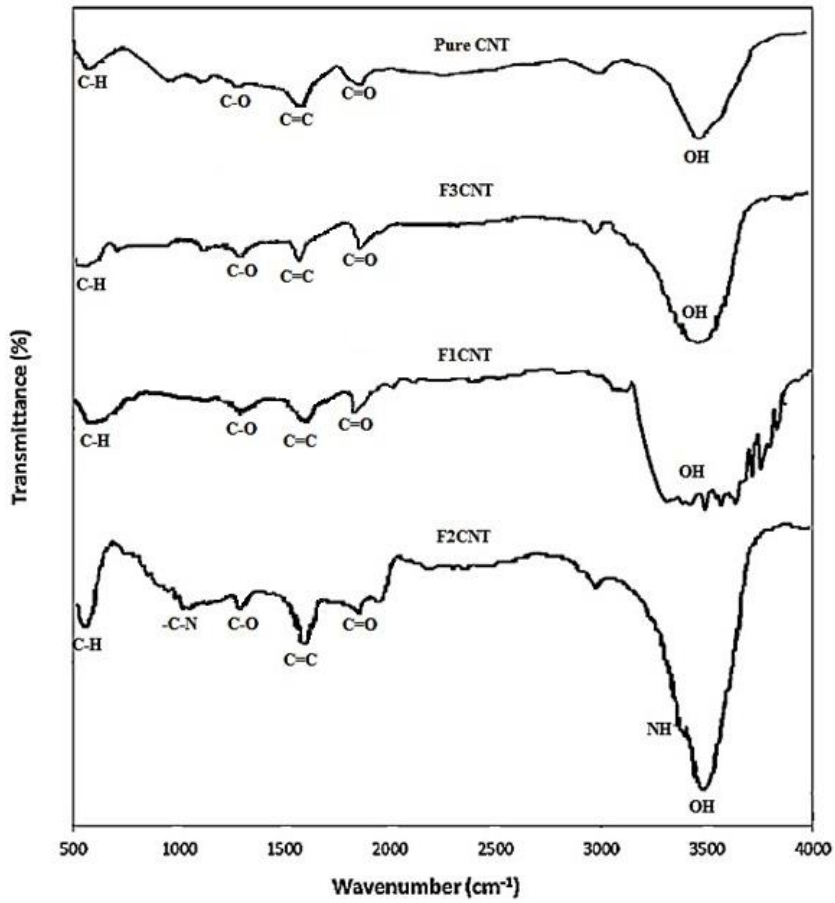

Figure 1. FTIR spectrum of common CNT and functionalized CNT support

CNT has a hydrophobic surface, which is prone to aggregation and precipitation in water. The above functionalized CNT can disperse easily in some protic and aprotic polar solvents such as water, ethanol and dimethyl formamide. There are certain numbers of carboxyl, hydroxyl, and amino groups on the outer walls that can form a hydrogen bond with polar solvents which improve CNT dispersion in solution. Figure 2 shows photographs of the CNT/dimethyl formamide solutions after 12 hr sonication. The common CNT settled down quickly in polar solvents, but the functionalized CNT stayed as a well dispersed solution for a number of days, without considerable change from their dispersion state. It was observed that a F2CNT has dispersed a bit better. This behavior confirms the FTIR spectrum.

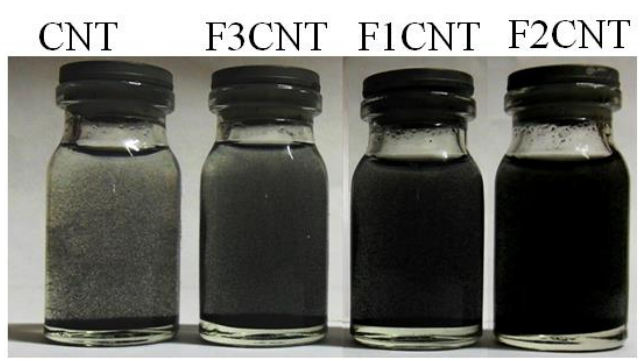

Figure 2. Dispersion photograph of common CNT and functionalized CNT after 48 hr

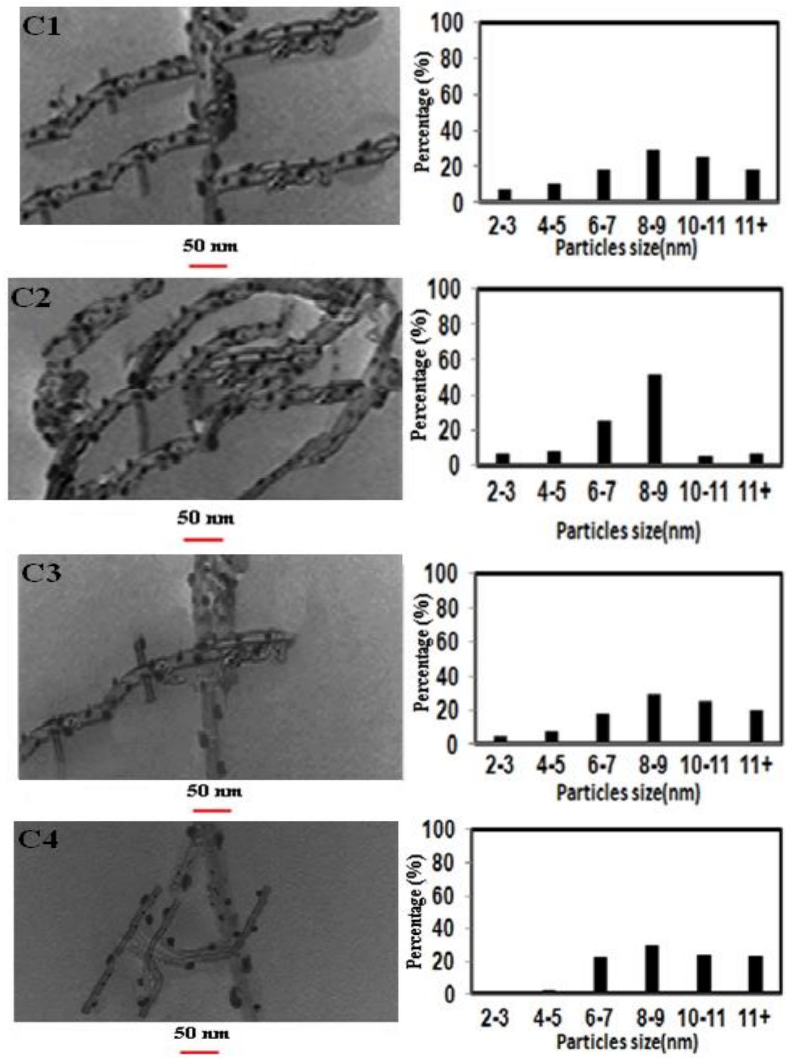

Figure 3. TEM images and particles size distributions for calcined catalysts

3.2. Catalysts characterization

The TEM images of the catalysts are shown in Figure 3. TEM images demonstrate the spreading of the particles inside and outside of the CNT channels. It seems that, capillary forces led to confinement of cobalt particles inside the CNT channels. This phenomenon can increase the cobalt dispersion of the catalysts [21, 31-35]. In the case of C_2 catalyst, the cobalt particles are dispersed mostly inside the tubes and the percentage of the particles lying at the outer surface of the functionalized CNT is lower compared to the other catalysts. The TEM images of the C_1-C_4 catalysts show that, the narrow inner diameter of the CNT (10 nm) restricted the insertion of particles in sizes close to the channels diameter. Almost all particles of sizes 10 nm and over are laying on the outer surface of the CNT walls.

Figure 3 also depicts the size distribution of the cobalt particles, which is determined using the population of cobalt particles on 5 different TEM pictures for each catalyst (about two hundred particles). This figure shows that cobalt nanoparticle size distributions for C_2 are better than other catalysts (C_1, C_3 and C_4). The functionalized CNT support enables to control a narrow cobalt nanoparticle size distribution, because the surface functional groups act as sites of interaction with metal precursor [13]. According to Figure 3, the average particle sizes for C_1-C_4 catalysts are about 10.7, 8.1, 10.9 and 11.4 nm and the standard deviation for the size distributions of cobalt particles are 1.25, 1.10, 1.3 and 1.5 nm respectively.

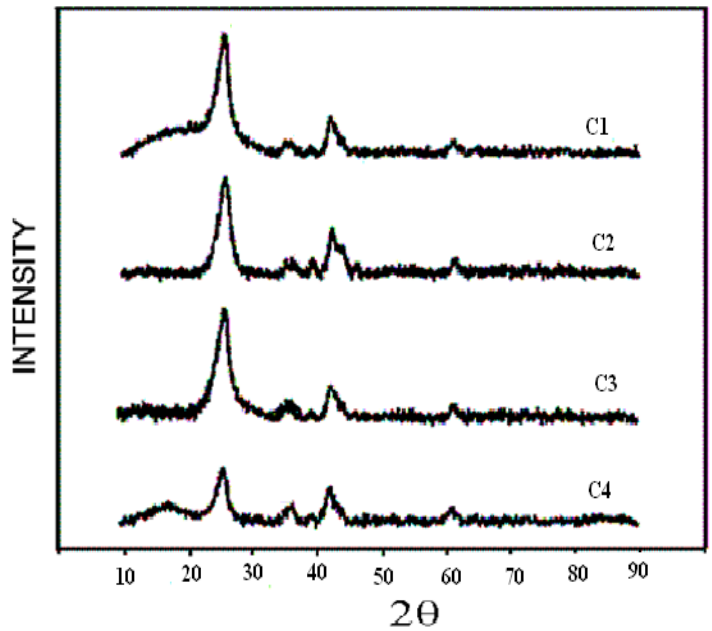

Figure 4. XRD patterns of calcined C1-C4 catalysts

XRD patterns of the calcined catalysts are shown in Figure 4. In the XRD spectra the peaks at 2θ values of 25° and 43° correspond to the CNT, while the other peaks in the spectra of the catalysts are related to different crystal planes of Co_3O_4 [13]. The peak at 2θ value of 36.8° is the most intense one of Co_3O_4 in XRD spectra of all catalysts. Minor peaks were also observed at 44°, and 52° for the catalysts which correlate with a cubic cobalt structure. This structure has no influence on the product selectivity [32].

Table 1 also shows the average Co_3O_4 crystal size of the catalysts calculated from XRD patterns using Scherer formula at 2θ value of 36.8° [36]. The average Co_3O_4 crystal size was determined after calcinations for the C_1-C_4 catalysts as approximately 15, 11.2, 16.4, 17.3 nm, corresponding to 11.25, 8.4, 12.3, and 12.95 nm when reduced to metal, respectively [36].

The results of hydrogen chemisorption tests are given in Table 1. As shown, functionalization of CNT considerably increased the hydrogen uptake and percentage dispersion. Maximum dispersion is achieved for C_2 catalyst. Also, the average particles diameter decreased, which are in agreement with the results of XRD and TEM tests. Also, the percentage reduction of the catalysts show a considerable increase. Therefore, it can be concluded that functional groups play an important role to dispersion and degree of reducibility of cobalt particles on the functional CNT cobalt catalyst supports. Higher dispersions and smaller cobalt cluster sizes in the case of the catalysts prepared by functionalized CNT will increase the number of sites available for CO conversion and hydrocarbon formation reactions rates.

Table1. H_2 chemisorption results and XRD cobalt crystal size for the calcined catalysts

Sample	μ mole H_2 desorbed /g cat.	μ mole O_2 consumed /g cat.	Reduction (%)	Dispersion (%)	XRD d_{Co3O4} (nm)	H_2-TPD d_{Co^O} (nm)
C_1	300	1350	57	11.08	15.0	10.7
C_2	347	1877	62	13.17	11.2	8.1
C_3	277	1198	54	10.67	16.4	10.9
C_4	251	1004	50	9.58	17.3	11.4

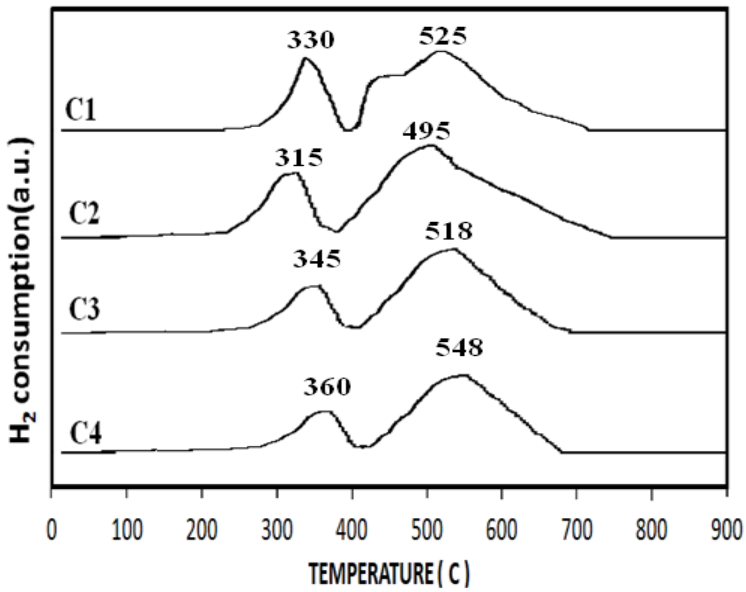

Figure 5. TPR patterns of calcined C_1 – C_4 catalysts from 30 to 900^{0}C.

The reducibility of the catalysts in H_2 atmosphere was determined by TPR experiments. The TPR spectra of the calcined C_1-C_4 catalysts and the specific reduction temperatures are presented in Figure 5. The low temperature peak (300–380^{0}C) is typically assigned to reduction of Co_3O_4 to CoO, although a fraction of the peak likely comprises the reduction of the larger, bulk-like CoO species to Co^o [21,32]. The second broad peak is assigned to reduction of small CoO to Co^o species, which also includes the reduction of cobalt species that interact with the support.

According to Figure 5, C_1-C_3 catalysts have shifted the reduction peaks to a lower temperature compared to that of the catalyst prepared on common CNT (C_4), indicating higher reducibility for cobalt particles deposited on functionalized CNT. Deposited cobalt particles of C_1-C_3 catalysts are easily reduced because of the confinement phenomenon and hydrogen spill-over of functional groups step [20,21].

4. Activity and product selectivity for FTS

Figure 6 shows the amount of %CO conversion, FTS rate, CO_2, CH_4, C_2-C_4 and C_5^+ selectivity for the different catalysts at steady state condition (after 144 hr FT synthesis). This figure shows that functionalization of the support noticeably increases the FTS rate and %CO conversion. The C_2 catalyst increased the %CO conversion from 30 to 47 compared to C_4 prepared on common CNT, while other functionalization method of support for C1 and C3 catalysts, increased the %CO conversion to 44 and 35 respectively. At the same time, FTS reaction rate (g CH/g cat/hr) increased to 0.2104, 0.2350, and 0.1791 for C_1-C_3 respectively, compare to C_4 catalyst with FTS rate of 0.1347. The results of catalyst characterization showed that the functionalization on CNT increased the catalyst reducibility, the metal dispersion, and decreased the average cobalt particle sizes. All these effects can be evidences for increasing the number of surface active cobalt sites and as a result the FTS reaction rate [8,19,22].

Also, it is well known that the exterior surfaces of the CNT are electron- rich, whereas the interior ones are electron deficient [15], which could influence metal and metal oxide particles in contact with either surface. The confinement of the nanoparticles (as shown in Figure 3) within the CNT, will lead to the particular interaction of the interior nanotubes surface with the metal particles, which favors the dissociative adsorption of CO. Since the chemisorption of reactants is the rate determining step on FTS reaction, one cobalt particle which is located inside the tubes must be more active than the one on the outer surface of the CNT. As mentioned, functionalization introduced a large number of functional groups on the nanotubes and increased the population of cobalt particles inside the tubes. The more active cobalt clusters inside the tubes can be another reason for CO conversion enhancement. The functional groups

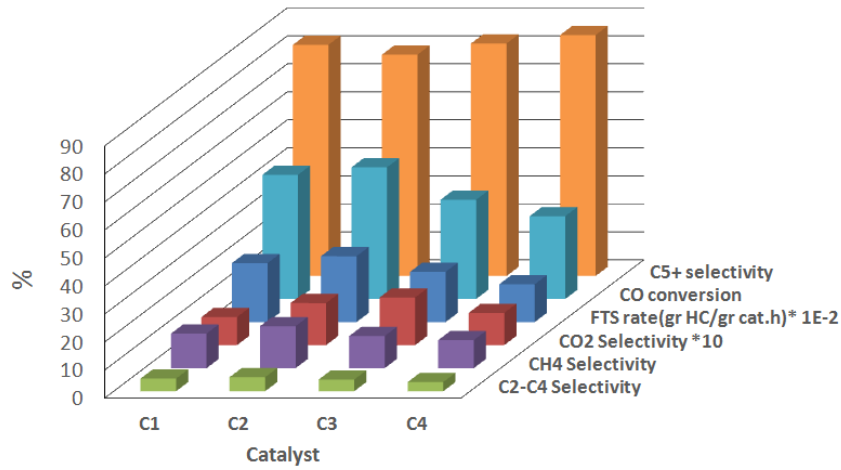

Figure 6. Catalytic performance of calcined C_1 – C_4 catalysts

also increase the adsorption of hydrogen on catalyst surface, which in turn leads to higher FTS rate [37]. Also theoretical studies on non-catalytic gas phase reaction have prefigured that confinement within small channels could increase the density of reactants, and hence create a locally higher pressure, which will favor syngas conversion to hydrocarbons in the case of functionalized CNT- supported cobalt catalysts [37].

Figure 6 also compares the hydrocarbon products distribution for all the catalysts at steady state condition (after 144 hr FT synthesis). As shown in this figure, methane selectivity is increased and liquid C_5^+ selectivity is decreased for functionalized CNT support catalysts. As mentioned before, functional groups will increase the amount of hydrogen adsorbed on the catalyst surface and then enhance the termination reactions to paraffin instead of chain growth to heavier hydrocarbons. The olefin to paraffin ratio for C_1-C_4 catalysts were 0.56, 0.48, 0.55 and 0.98 respectively. Lower amount of olefin to paraffin ratio in the final products of C_1-C_3 (Specially C_2) catalysts confirms higher rate of termination reactions to paraffins.

4.1. Stability of FTS catalysts

Figure 7 shows the variations of CO conversion with the time on stream (TOS) for C_2 and C4 catalysts. The catalysts reached their highest activity within 12 hr. Afterward, they showed different stability pattern within a time period of 144 hr. Figure 7 shows that C_2 catalyst supported on the functionalized CNT is more stable that C4. In the case of C_2, syngas conversion drops slowly from a high conversion of 55% at TOS of 12 hr to 54% at TOS of 144 hr. At the same time, the percentage CO conversion for C_4 catalyst decreased from 36% to 32.4%. One of the major factors for catalyst deactivation is metal site agglomeration or sintering, during FT reactions. The stability of the catalyst may be attributed to the extent of functional groups and defects and/or the structure of CNT support. The defects on the surface work as anchoring sites for stable metal particles on the supports surface [20].

Table 2. Textural properties, and cluster sizes of the N-doped functionalized CNT and CNT-supported cobalt catalysts after 140 hr reaction

Catalyst		BET surface Area (m^2/g)	Total pore volume (ml/g)	Average pore diameter (Å)	XRD d_{Co3O4} (nm)
C_2	Befor reaction	304.0	0.85	110.0	15.2
	After reaction	303.5	0.85	109.8	15.2
C_4	Befor reaction	133.0	0.42	121.0	17.3
	After reaction	130.7	0.37	118.5	18.1

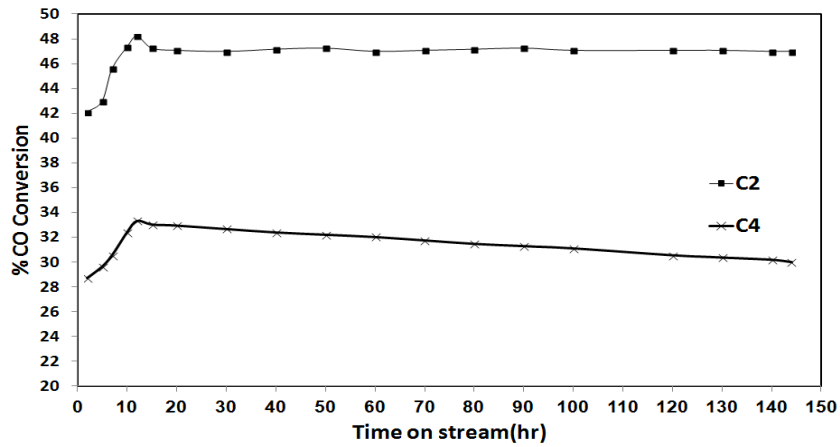

Figure 7. CO conversion variations with time on stream for C_2 and C_4 catalysts

Table 2 reports the variations of pore size and BET surface area and XRD results (Patterns are not shown here) of C_2 and C_4 catalysts after the FTS reaction within a time period of 144 hr. According to this table the particle size, pore size, and BET surface area of C_2 catalyst didn't show a sensible change. The stability of the catalyst may be attributed to the extent of functional groups which prevented metal site agglomeration or sintering, and unavailability of some active sites due to pore blockage.

5. Conclusion

This research has been carried out using functionalized CNT supported cobalt catalysts to compare the effects of different functional groups on activity, selectivity and stability of catalysts with cobalt loading of 15 wt.%. TPR results showed that, deposition of cobalt nanoparticles on the functionalized CNT, shift the reduction steps to a lower temperatures and the reducibility of the catalysts improved significantly, compared to the catalyst prepared on common CNT. According to TEM analysis, N-doped functionalized CNT support shows a narrow particle size distribution. For the CNT supports with open cap, capillary forces led to confinement of small cobalt particles inside the CNT channels, which interact with inner wall of the CNT and favors the reduction of Co_3O_4 species. Functionalized CNT as a catalyst support of cobalt nanoparticles increase metal–support interaction, but maintains high dispersion and reducibility of cobalt, which can be attributed to hydrogen spill-over and promotional effect of functional groups on CNT surface. Normally, this will not occur in catalyst prepared on CNT or with small particles supported on oxidic carriers. It was also found that FTS activity and selectivity of the catalysts are strongly dependent on the size distribution of the cobalt clusters. However, the particle's confinement within functionalized CNT may be more important than the particle size effect for the CO conversion and FTS activity and selectivity. Thus, improvement of the uniformity of the catalyst particles supported on functionalized CNT, leads to a better CO conversion, FTS activity, compared to that prepared on common CNT support. Functional groups also decreased the sintering of cobalt nanoparticles and affect the stability of catalyst during the FTS reaction. This new catalyst preparation method may offer an attractive alternative for nanoparticles synthesis with uniform, and various size distributions for fundamental catalytic studies especially such for structure-sensitive FT catalysis.

References

1. Y. Khodakov, W. Chu, P. Fongarland, Chem. Rev., 107, 1692 (2007).
2. M.E. Dry, Catal. Today, 71, 227 (2002).
3. A. Jager, R. Espinoza, Catal. Today, 23, 17 (1995).
4. D.M. Guldi, Nature, 447, 50 (2007).
5. J. J. Niu, J.N. Wang, Y. Jiang, L.F. Su, J. Ma, Microporous Mesoporous Mater., 100, 1 (2007).

6. W. Chu, L.N. Wang, P. A. Chernavskii, A. Y. Khodakov, Angew Chem. Int. Ed., 47, 5052 (2008).
7. R. M. Malek Abbaslou, J. Soltan, A. K. Dalai, Appl. Catal. A: General, 379, 129 (2010).
8. B. Bhushan, Springer Handbook of Nanotechnology, 68 (2007)
9. M. R. LaBrosse, W. Shi, J. K. Johnson, Langmuir, 24, 9430 (2008).
10. L. F. Mabena, S. Sinha Ray, S. D. Mhlanga, N. J. Coville, Appl. Nanosci., 1, 67 (2011).
11. P. J. Berge, V. D. Loosdrecht, S. Barradas, V. D. Kraan, Catal. Today, 58, 321 (2000).
12. G. Jacobs, T. K. Das, Y. Zhang, J. Li, G. Racoillet, B. H. Davis, Appl. Catal. A, 233, 263 (2002).
13. G. L. Bezemer, A. Van Laak, A. J. Van Dillen, K. P. De Jong, Stud. Surf. Sci. Catal., 147, 259 (2004).
14. A. Tavasoli, A. M. Rashidi, K. Sadaghiani, A. Karimi, A. A. Khodadadi, Y. Mortazavi, European Patent EP 1782885 (2007).
15. A. Tavasoli, K. Sadagiani, F. Khorashe, A. Seifkordi, A. Rohani, A. Nakhaeipour, Fuel Proc. Tech., 89, 491 (2008).
16. A. Tavasoli, R. M. Malek Abbaslou, M. Trepanier, A. K. Dalai, Appl. Catal. A, 345, 134 (2008).
17. T. G. Ros, A. J. Van Dillen, J. W. Geus, D. C. Koningsberger, Chem. Eur. J., 8, 1151 (2002).
18. H. P. Boehm, Adv. Catal., 16, 179 (1966).
19. F. Rodríguez-Reinoso, Carbon, 36, 159 (1998).
20. Y. Zhang, Y. Liu, G. Yang, Y. Endo, N. Tsubaki, Catal. Today, 142, 85 (2009).
21. A. Karimi, B. Nasernejad, A. M. Rashidi, A. Tavassoli, M. Pourkhalil, Fuel, 117, 1045 (2014).
22. H. P. Boehm Carbon, 32, 759 (1994).
23. A. Tavasoli, S. Taghavi, J. of Energy Chem., 22, 747 (2013).
24. A. M. Rashidi, A. Nouralishahi, A. A. Khodadadi, Y. Mortazavi, A. Karimi, K. Kashefi, Int. J. Hydrogen Energy, 35, 9489 (2010).
25. F. Li, H. M. Cheng, Y. T. Xing, P. H. Tan, G. Su, Carbon, 38, 2041 (2000).
26. R. Andrews, D. Jacques, D. Qian, E. C. Dickey, Carbon, 39, 1681 (2001).
27. M. Zhang, M. Yudasaka, S. Iijima, J. Phys. Chem. B, 108, 149 (2004).
28. H. Naeimi, A. Mohajeri, L. Moradi, A. M. Rashidi, Appl. Surf. Sci., 256, 631 (2009).
29. S. Kundu, W. Xia, W. Busser, M. Becker, D. A. Schmidt, M. Havenith, M. Muhler, Phys. Chem. Chem. Phys., 12, 4351 (2010).
30. A. Karimi, B. Nasernejad, A.M. Rashidi, Korean J. Chem. Eng., 29, 1516 (2010).
31. S. Murugesan, K. Myers, V. Subramanian, Appl. Catal. B: Environmental, 103, 266 (2011).
32. M. Trepanier, A. Tavasoli, A. K. Dalai, N. Abatzoglou, Appl. Catal. A, 353, 193 (2009).
33. W. Chen, Z. Fan, X. Pan, X. Bao, J. Am. Chem. Soc., 130, 9414 (2008).
34. R. M. Malek Abbaslou, A. Tavasoli, A. K. Dalai, Appl. Catal. A: General, 355, 41 (2009).
35. X. Pan, Z. Fan, W. Chen, Y. Ding, H. Luo, X. Bao. Nature, 6, 507 (2007).
36. A. Karimi, A. Nakhaei Pour, F. Torabi, B. Hatami, M. Alaei, M. Irani, J. Nat. Gas Chem., 19, 503 (2010).
37. M. Trepanier, A. Tavasoli, A.K. Dalai, N. Abatzoglou, Fuel Proc. Tech., 90, 367 (2009).